LROC NAC GLOBAL PHOTOMETRY: TERRAIN TYPES AND PHASE CURVES. A. K. Boyd[1] (aboyd@ser.asu.edu) and M. S. Robinson [1], [1]Arizona State University SESE, Tempe, AZ.

Introduction: Lighting conditions beneath the Lunar Reconnaissance Orbiter (LRO) systematically vary from month-to-month providing the opportunity to characterize photometric properties across a broad range of surface materials. Off nadir campaigns and multi-temporal imaging allow observations with phase angles ranging from 0° to 110° (smaller range at high latitudes). As a result, the Lunar Reconnaissance Orbiter Camera (LROC) Narrow Angle Camera (NAC) has acquired a robust set of broadband (450 - 700 nm), globally distributed, photometric observations.

Each NAC has a 2.85° field-of-view [**1**], thus the phase angle (angle between the emission and incidence vectors) changes little in one NAC image while the incidence (angle of sub-solar vector relative to the surface normal) and emission (angle of camera boresight vector relative to the surface normal) angles [**2**] vary dominantly from topography (in a single image). To allow quantitative comparisons of reflectance values from spatially dispersed NAC images, we derived empirical photometric solutions from NAC image tiles (similar to the method described in [**3,4,5**]), but with a new photometric function and more LROC NAC images sampled at smaller pixel scales than the previous work. We call these solutions the Mean Moon Photometric Functions (MMPFs).

$$LS = \frac{\cos(i)}{\cos(i) + \cos(e)}$$

$$\frac{I}{F} = LS \cdot e^{\left[a_0 g^2 + a_1 g + a_2 g^{\frac{1}{2}} + a_3 \cos(e) + a_4 cos(i) + a_5 \cos^2(i)\right]}$$

Equation 1: MMPF with 6 free variables. The Lommel-Seeliger correction is applied with a 2nd degree exponential dependent on phase (g), emission (e), and incidence (i) angles.

Methods: The globe was divided into ten compositional and maturity units using optical maturity (OMAT) values [**6**], TiO2 content [**7**], and a mare boundary shapefile [**8**]. To compute (MMPFs) including Mature Highlands (MH), Immature Highlands (IH), Mature Mare (MM), and Immature Mare (IM), data from 1km x 1 km NAC tiles were reduced similar to the method described in [**5**].

LROC NAC images were selected based on incidence angle (<91°) and emission angle (<91). Only images with data quality IDs < 16 and exposure times <2 ms were included in the study.

A linear least squares fit was achieved for the MMPFs by fitting to the response variable, log(I/F), using the dependent variables g, cos(e), and cos(i).

Data Preparation: Radiometrically calibrated I/F [**9,10**] NAC images were binned to 1 km x 1 km pixel scales enabling accurate photometric angle calculations from the GLD100 [**11**], while maintaining a manageable dataset. Photometric angles (phase, local emission, and local incidence angles), latitude, and longitude were calculated for each tile.

Curve Fitting: The resulting dataset was binned by photometric angles (1° bins) and the median for each bin was used for fitting thus removing the bias of higher point density regions near nadir and at larger incidence angles.

The preliminary and final fittings were performed with emission and incidence angles <85° and all phase angles. After the preliminary fitting, the normalized I/F was computed for all input data points, and outliers were identified as points greater than 3σ from the mean normalized I/F of the terrain. With outliers excluded, the median for each bin was recomputed, and the functions were fit again using the bins.

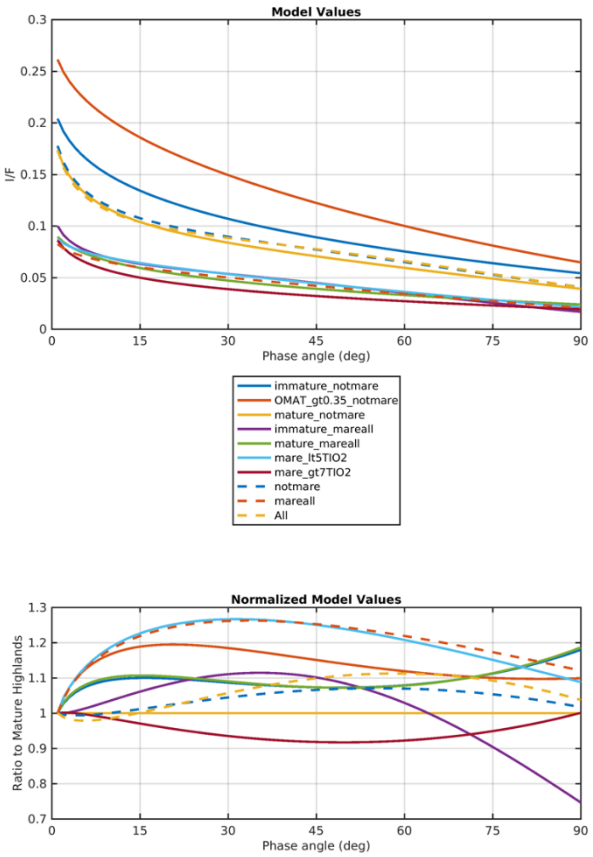

Fig. 1 *Photometric models are compared to investigate surface property and compositional differences across different terrains. The highlands are more backscattering than the mare, and the mature highlands have the narrowest opposition curve of the terrains investigated.*

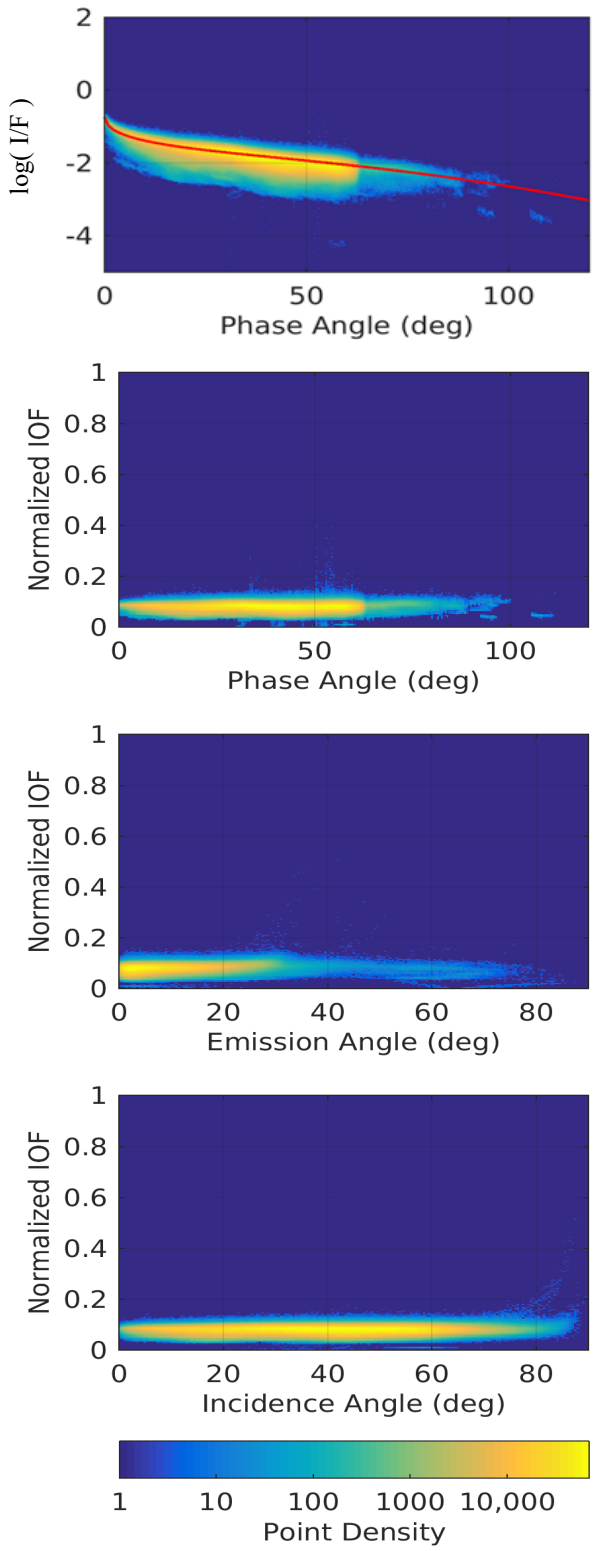

Fig. 2 *residuals mature highland. a) log(I/F) vs phase angle with the model drawn in red. b-d) Normalized I/F vs. photometric angle.*

Results and Discussion: The MMPF is designed as a general-purpose correction for the Moon with care taken to create a smooth function while balancing the number of free parameters. The function is well fit for phase angles < 120° and emission and incidence angles <85°; roughly 93% of all illuminated NAC images within 60° latitude of the equator. The solution presented here is improved upon that of [**5**] by fit accuracy due to significantly more observations and a new photometric function.

Residuals: At phase angles <10° the normalized I/F remains flat toward 0° (**Fig. 1B**), showing that the MMPF adequately describes the opposition surge [**2**]. Normalized I/F departs slightly from the horizontal fit as emission angle approaches 35° (**Fig. 1C**). For nadir images, the departure is due to steep slopes (>25°), which are composed of immature material with higher reflectance. (**Fig. 1C**). Normalized I/F is horizontal out to 85° incidence angle (**Fig. 1D**), beyond which the presence of shadows due to km scale topographic facets begins to dominate the reflectance.

Terrains: High OMAT (immature) non-maria has the highest reflectance and high TiO_2 maria (for all OMAT) has the lowest reflectance of all terrains. The high TiO_2 maria is the only region that is more backscattering than mature highlands. The immature maria is the most different from mature being the most isotropic, while the maria <5 wt% TiO_2 and the least mature areas of the highlands (OMAT >0.35) exhibit the broadest opposition surge.

The mature highlands have the narrowest opposition surge, which is interpreted to mean that the mature highlands have the most well developed regolith and fairy castle structure. However, the broadening of the opposition surge in the immature highlands (OMAT > 0.2) indicates larger grain sizes and less internal scatterers.

The more isotropic (less backscattering) nature of the immature maria is interpreted as fewer scatterers in the grains and/or higher absorptions in grains than other terrains. The highly backscattering TiO_2 maria is thought to be due to the amount of opaque materials.

References: [**1**] Robinson et al. (2010) *Space Sci. Rev.* 150: 81-124. [**2**] Hapke B. (2012) Cambridge Univ. Press. [**3**] Boyd et al. (2014) *LPSC 45*, #2826. [**4**] Boyd et al. (2017) *3rd Planet. Data Workshop,* #1986 [**5**] Boyd et al. (2018) *LPSC 49*, #2671. [**6**] Lucey et al. (2000) *JGR,* 105 [**7**] Sato et al. (2017) *Icarus*, 296 [**8**] Nelson et al. (2014). *LPSC 45*, #2861 [**9**] Becker, K.J., et al. (2013) *LPSC 44*, #2829 [**10**] Humm, D. C. et al. (2016) *Space Sci. Rev.*, 200. [**11**] Scholten, F. et al. (2012). *JGR*, 117.